Vol. 17, No. 2 (2018) 707-721
Revista Mexicana de Ingeniería Química

FLUID DYNAMICS AROUND FLAT-END CYLINDRICAL QUENCH PROBES UNDER ISOTHERMAL AND NON-ISOTHERMAL CONDITIONS

DINÁMICA DE FLUIDOS ALREDEDOR DE PROBETAS CILÍNDRICAS DE BASE PLANA, TEMPLADAS BAJO CONDICIONES ISOTÉRMICAS Y NO ISOTÉRMICAS

A. Cervantes-García[1], G. Solorio-Díaz[1]*, H.J. Vergara-Hernández[2], B. Hernández-Morales[3]

[1] *Facultad de Ingeniería Mecánica, Universidad Michoacana de San Nicolás de Hidalgo. Santiago Tapia 403, Centro, Morelia, Michoacán, 58000, México.*

[2] *División de Estudios de Posgrado e Investigación, Instituto Tecnológico de Morelia. Av. Tecnológico 1500, Lomas de Santiaguito, Morelia, Michoacán, 58120, México.*

[3] *Facultad de Química, Departamento de Ingeniería Metalúrgica. Universidad Nacional Autónoma de México, Circuito Interior s/n, México, DF 04510, México.*

Received November 1, 2017; Accepted February 28, 2018

Abstract

The most common methodology to describe the complex phenomena occurring during quenching operations is based on measuring cooling curves inside metal test probes instrumented with thermocouples. There are many variants regarding specimen shape, although the preferred shape is a flat-end cylindrical probe. However, mathematical and physical modeling studies, carried out under isothermal conditions, regarding the hydrodynamic behavior of the quenchant around flat-end cylindrical probes suggest that this type of probe should not be recommended for studies quenching. In this paper, we study fluid dynamics around an instrumented flat-end cylindrical probe, both under isothermal (un-heated probe) and non-isothermal conditions (probe heated to 900 ºC and cooled in water at 60 ºC). For this purpose, water at 60 ° C was used as cooling fluid; three free-stream water velocities (0.2, 0.4 and 0.6 m/s) were studied. Visualization techniques using a high-speed camera and optical filters were applied to characterize the flow around the probe and, at the same time, thermal histories were measured within the probe. The results show that fluid dynamics under non-isothermal conditions is very different from that under isothermal conditions; therefore, it is not advisable to directly correlate fluid dynamics around metal probes characterized under isothermal conditions with cooling curves or the evolution of the wetting front during an actual quench.

Keywords: quenching, cooling curves, flat-end cylindrical probe, wetting front, fluid dynamics.

Resumen

La metodología más común para describir los fenómenos complejos que ocurren durante las operaciones de temple se basa en la medición de curvas de enfriamiento. Existen variantes de la forma de la probeta, aunque la forma preferida es cilíndrica de base plana. Sin embargo, estudios de modelado físico y matemático realizados en condiciones isotérmicas respecto al comportamiento hidrodinámico del fluido de temple alrededor de las probetas cilíndricas de base plana, sugieren que este tipo de probetas no es recomendable para estudios de temple. En este artículo, se estudia la dinámica de fluidos alrededor de una probeta cilíndrica de base plana bajo condiciones isotérmicas (probeta sin calentar) y no-isotérmicas (probeta calentada a 900 ºC y enfriada en agua a 60 ºC). Para este propósito, se usó agua a 60 °C como fluido de enfriamiento; se estudiaron tres valores de velocidad de corriente libre (0.2, 0.4 y 0.6 m/s). Se utilizó una cámara de alta velocidad y filtros ópticos para caracterizar el flujo alrededor de la probeta y, al mismo tiempo, se midieron historias térmicas al interior de la misma. Los resultados muestran que la dinámica de fluidos en condiciones no-isotérmicas es muy diferente a la que ocurre en condiciones isotérmicas; por consiguiente, no es aconsejable correlacionar la dinámica de fluidos en condiciones isotérmicas, con curvas de enfriamiento o con el frente de mojado en un temple real.

Palabras clave: temple, curvas de enfriamiento, probeta cilíndrica de cara plana, frente de mojado, dinámica de fluidos.

* *Corresponding author. E-mail*: gdiaz@umich.mx
Tel. +52 1 443 3223500 ext.116
doi: 10.24275/10.24275/uam/izt/dcbi/revmexingquim/2018v17n2/Cervantes
issn-e: 2395-8472

1 Introduction

Millions of dollars are spent each year because of distortion, fracture and low mechanical properties due to unexpected problems during quenching processes. The non-uniformity in the heat transfer of the rapidly cooled parts is perhaps what most contributes to these problems. The Jominy end quench hardenability test has been used to predict the mechanical properties of the quenching metallic components (Smoljan, 2006). Some studies use empirical hardness-microstructure correlations and the numerical solution of heat transfer using the inverse heat conduction method to predict the hardness profile along steel specimens (López-Martínez *et al*, 2013). However, it is not possible to achieve the desired as-quenched properties of a metallic material, unless there is an accurate knowledge of the heat transfer between the hot metal and the quenching fluid (Tensi *et al*., 1985). To characterize the effectiveness of the various quenching fluids, it is necessary to quantify the influence of the boiling phenomena that take place during the quench on the cooling rate history. One of the factors strongly affecting the uniformity of heat transfer is the flow pattern around the parts (Owaku, 1992; Kern, 1985; Tensi *et al*., 1997; Long, 1994; Tensi *et al*., 1995), which generates large temperature gradients within the part (Narazaki *et al*., 2002).

Three sequential stages have been identified when a hot part is quenched in a subcooled liquid (Tensi and Stich, 1992; Stich and Tensi, 1995): (a) film boiling, that occurs at high surface temperature values and is characterized by the formation of a continuous vapor film around the probe. The vapor film acts as a resistance to heat transfer towards the bulk of the subcooled liquid and affects the cooling rate history to the point of favoring the formation of unwanted microconstituents, thus reducing the mechanical properties of the material; (b) nucleate boiling, associated with high heating rates due to the formation of bubbles that remove large amounts of heat; and (c) pure convection (either natural or forced), i.e., without boiling, during which heat extraction diminishes towards zero. Additionally, in the quenching literature the occurrence of a so-called shock-boiling regime just before a stable vapor film forms has been reported (Kobasko *et al*., 1997); it usually occurs during the first 0.1 s after the heated probe is submerged in the quenching medium. Through experiments involving heating of metallic parts in a subcooled liquid, a transition zone, characterized by the coexistence of film boiling and nucleate boiling, has been identified (Nukiyama and Shiro, 1966; Shiro and Nukiyama, 1984). The onset of this regime is known as the Leidenfrost point. Leidenfrost described the term wetting in the 1950?s and associated it with a single value of temperature at the part surface such that above it the vapor film is completely stable (Leidenfrost, 1756). As mentioned before, from the viewpoint of industrial quenching operations, the occurrence of the film boiling stage delays the cooling process, which is undesirable and has led to the implementation of agitation of the quenchant to promote the collapse of the vapor film; therefore, the heat transfer process, as applied in industry, may be described as forced convective quenching. In non-stationary processes such as quenching, local boiling phenomena are a function of time and position along the probe (Kunzel *et al*., 1986). This behavior leads to the occurrence of a wetting front, which is the loci of the boundary between the vapor film and the occurrence of film boiling (Tensi *et al*., 1997). The evolution of the wetting front, i.e., the wetting front kinematics largely determines the thermal field evolution during quenching and, therefore, must be carefully characterized.

Cooling curve analysis has been accepted as the most useful methodology to describe quenching and has been used for evaluation of various quenchants (Bodin and Segerberg, 1992). Cooling curves are usually obtained quenching a test probe and measuring the temperature as a function of time at a specified point within the specimen. From the temperature-time curve, a cooling rate-time curve can be calculated. The test probes may be cylinders, plates or spheres. There are many variants of the specimen shape, size and materials, though the preferred shape is a flat-end cylindrical probe (Totten *et al*., 1993; Totten *et al*., 2009; Hernández-Morales *et al*., 2011). In addition to ISO 9950 (1995), several standards have been developed including ASTM D6200-01 (2012), ASTM D6482-06 (2011), and ASTM D6549-06 (2011), which are all based on a 12.5 mm diameter by 60 mm cylindrical Inconel 600 probe with a Type K thermocouple inserted at the geometric center. Other standard probes are constructed using aluminum alloys or silver with a thermocouple at the geometric center, such as ASTM D7646-10 (2010), with the thermocouple positioned at the surface, such as that described in Method A of JIS K 2242 (2012), or a silver probe with a center thermocouple.

Several studies have been carried out using flat-end cylindrical probes to estimate the heat transfer boundary condition or to characterize the evolution of the wetting front (Narazaki, *et al*., 2004; Lübben *et al*., 2011). Other researchers have used variations of this probe. Narazaki *et al*. (1989 and 1996) have shown results comparing the performance of flat-end, rounded-edge and hemispherical-end cylindrical probes cooled in an agitated bath. Based on the reproducibility of the cooling curves they concluded that the best probe would be that with the hemispherical-end. He found, under isothermal conditions, that the flow around a cylindrical probe with hemispherical ends is laminar except around the upper end, while the flow around a flat-end cylindrical probe is turbulent with vortices which could influence the accuracy and reproducibility of the cooling curve test results.

Studies conducted by Vergara-Hernández and Hernández-Morales (2009) and Vergara-Hernández *et al*. (2010) pointed out that the hydrodynamics of the quenchant around the probe plays a significant role in defining the geometry of the vapor film as well as wetting front kinematics during forced convection quenching. They concluded that the wetting front is not symmetric when flat-end cylindrical probes are used (even for fully developed flow and relatively low values of quenchant velocity). Computer simulation of the vorticity field near the base of the probe (considering an isothermal system at ambient temperature) showed that there is a significant vorticity gradient which may favor the chaotic collapse of the vapor film and the formation of an asymmetric wetting front which in turn complicates the study of the wetting front kinematics. Therefore, they proposed a conical-end cylindrical probe, which ensured that the vapor film collapsed uniformly around the probe because the formation of the wetting front was concentrated, initially, at the probe tip.

Ramezanzadeh *et al*. (2017) numerically investigated forced convection quenching process of hot pieces in subcooled liquid quenching oil at different inlet velocities in the range of 0.1-0.6 m/s. The model assumed laminar flow in all cases. Instead of using a database for the Leidenfrost temperatra, the liquid -vapor interface was tracked using the Volume of Fluid method. They found that rewetting depends entirely on inlet velocity; the higher velocities produced unwanted vorticity that resulted in a highly non-uniform temperature distribution.

In those papers it has been proposed that flat-end cylindrical probes are not a good option to estimate the heat transfer boundary condition or to characterize the evolution of the wetting front because the flow around a flat-end cylindrical probe is turbulent with vortices which could influence the accuracy and reproducibility of the cooling curve test results. However, the characterization of the fluid dynamics around flat-end cylindrical probes, using experimental techniques or numerical simulations, has always been performed under isothermal conditions (unheated probe) (Vergara-Hernández, and Hernández-Morales, 2009; Vergara-Hernández *et al*., 2010; Tensi *et al*., 2000; Maniruzzaman and Sisson, 2001; Hernández-Morales *et al*., 2011), a situation that may lead to erroneous conclusions. Given that the flat-end cylindrical probe is the most common geometry featured in the different standardized norms, it is important to be able to determine the dynamics of the cooling fluid around this type of probe under non-isothermal conditions (probe heated to 900 ºC and cooled in water at 60 ºC).

Lee *et al*. (2017) carried out experiments to characterize heat extraction during forced immersion. In particular, they quench a hot steel block uniformly heated to 900 ? while registering cooling curves and video-recording boiling phenomena using a color high-speed CCD camera. The visualization showed that surface wetting at the lateral surface starts from the bottom due to the flow separation from the top-edge.

The goal of this paper is to characterize, by means of visualization techniques based on video-recordings using a high-speed camera and wavelength filters of the visible spectrum together with measured local thermal histories, the fluid dynamics around flat-end cylindrical probes, both under isothermal and non-isothermal conditions, and to determine its effect on the behavior of the vapor film, the evolution of the wetting front and the local cooling rate history.

2 Experimental work

The experimental work was designed to: 1) produce direct observations of the film boiling and the wetting front; 2) visualize streamlines within the fluid; and 3) calculate local cooling rate histories. Fig. 1 shows a schematic of the experimental setup. Water flows from a tank into a 44 mm inside diameter plexiglass tube at a controlled flow rate such that the free-stream velocity is known and the flow is fully developed.

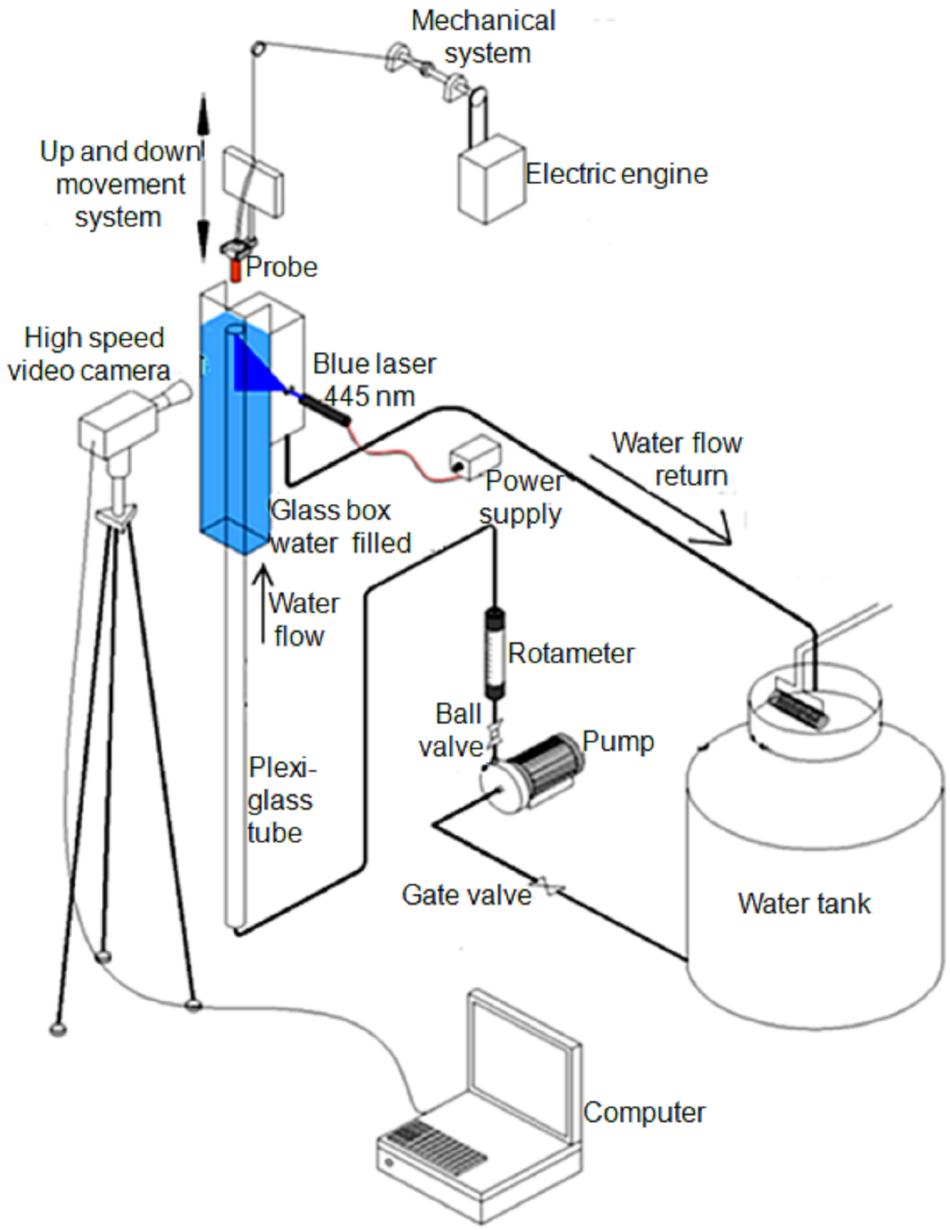

Fig. 1. Schematic representation of the experimental set-up.

In non-isothermal tests, the probe is heated in an electric resistance furnace and then transferred to the test position within the plexiglass tube.

The experimental design is based on Vergara-Hernández and Hernández-Morales (2009), improving the transferring of the probe from the furnace to the test position with the aid of an electric motor, achieving a constant immersion velocity of the probe in each one of the experiments. The water recirculation system was also redesigned to reduce the effect of turbulence upon contact of the probe with the flowing water. To avoid image distortion, a section of the plexiglass tube was surrounded by a hollow rectangular prism case fabricated with glass and filled with water. The streamlines were visualized using 50 mm-diameter polyamide particles, a blue laser of 2 W with a wavelength of 445 nm, and a high-speed camera (Photron, model PCI R2) capable of obtaining up to 1000 frames per second.

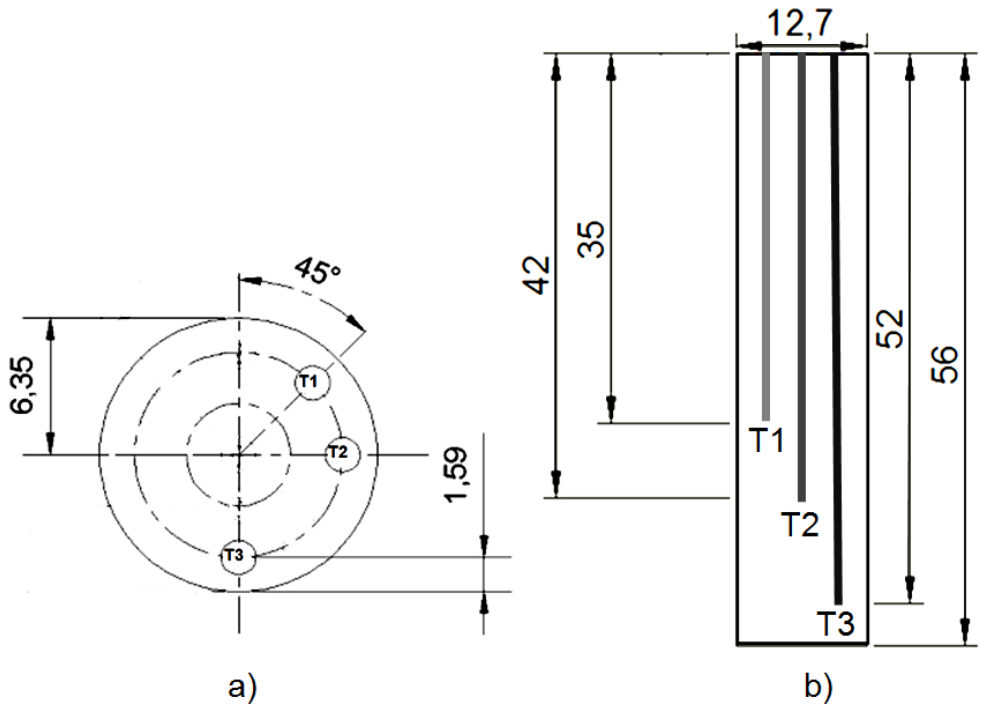

Fig. 2. Axial and radial position of the thermocouples within probe (distances in millimeters): a) top view, b) side view.

The water was seeded with the polyamide particles, which were illuminated by the laser sheet and their position recorded with the high-speed camera. The high-speed camera was also used to capture detailed images of the instantaneous flow patterns and to reveal instantaneous oscillating flow around the probe. A Navitar Macro Zoom 7000 was used with the high-speed camera to magnify the image close to the probe; it is a close-focusing (6X) macro video lens which is versatile and specifically designed to be used in applications where objects under 1-inch diameter must be imaged.

For the non-isothermal experiments, a short-pass optical filter (400-550 nm transmission wavelength, 85% transmission) was used to block light with wavelengths higher than 550 nm; as a result, better suited images were obtained with the filter because refraction of light emitted by the probe is avoided. These optical filters may also be used as hot mirrors to minimize unwanted heat caused by infrared radiation.

Fig. 2 shows the flat-end cylindrical probe. The probe was machined from AISI 304 stainless steel stock bar; since this is an austenitic stainless steel, no phase transformation will occur during quenching. The probe was instrumented with three 1.58 mm-dia., Inconel sheathed, type-K thermocouples. The thermocouples were placed at the same radial position, but at different axial positions; they were press-fitted to attach them to the probe. The thermocouple placement was designed to achieve two objectives: 1) to facilitate comparison between the thermocouple response and the video-recording and 2) to allow characterization of the evolution of the wetting front along the probe length.

The probe was heated to 915 °C in an electrical resistance furnace without protective atmosphere. Once the probe reached the required temperature in the furnace, the latter was removed and the probe quickly immersed in the upper portion of the plexiglass tube in which water at 60 ºC was flowing; the water flow-rate and temperature had been previously stabilized. Considering transfer from the furnace to the test position, the initial test probe temperature is 900 °C.

The camera was placed in front of the tube at the probe quenching position, approximately 50 cm from the tube external wall, and it was carefully positioned at 90° with respect to the laser sheet. The actual rate of capture was 60 frames per second, which allowed a resolution of 512 x 480 pixels.

Table 1. Experimental conditions.

Probe geometry	Flat-end cylindrical Probe
Probe material	AISI 304 stainless steel
Initial test temperature	900 °C
Quenchant	Water
Quenchant temperature	60°C
Quenchant velocity	0.2, 0.4, 0.6 m/s.
Reynolds number (Re)	18,526 (with 0.2 m/s)
	37,052 (with 0.4 m/s)
	55,577 (with 0.6 m/s)

Images were computed using the PIVlab Software (Thielicke *et al.*, 2014) applying Line Integral Convolution (LIC) and Cross Correlation to compute streamlines and velocity vectors, respectively. To record the thermal response, the three thermocouples were connected to a computer-controlled data acquisition system (IOTECH, model TempScan1000). ChartView 1.02 was used to control the data acquisition operation; a data acquisition frequency of 10 Hz was used for all experiments.

Table 1 shows the experimental conditions. The quenchant velocity is the free-stream water velocity inside the plexiglass tube, *i.e.*, before reaching the probe position. The Reynolds number is calculated with Eq. 1:

$$Re = \frac{\rho V D}{\mu} \tag{1}$$

Where ρ is the fluid density, V is the average velocity, D is the hydraulic diameter and μ is the dynamic viscosity; Re is calculated for a water temperature of 60 ºC.

3 Results

3.1 Fluid dynamics

Fluid dynamics around the flat-end cylindrical probe is described using streamlines computed from images extracted from the video-recordings and velocity fields obtained through PIV measurements. Fig. 3 shows images extracted from the video-recordings, streamlines and velocity fields around the flat-end cylindrical probe for the three values of free-stream water velocity studied (0.2, 0.4, and 0.6 m/s) under isothermal conditions (probe at room temperature inside a plexiglass tube with water flowing at 60°C). Results from the experiment with a free-stream water velocity of 0.2 m/s (see figs. 3 a) and 3 d)) show streamline separation at the leading edge of the flat-end cylindrical probe. The boundary layer is unable to follow the sharp vertex, losing energy, leading to separation; also, a recirculation zone is formed, due to an adverse pressure gradient, with small-scale vorticity. The velocity fields and the streamlines show that the separation of the water boundary layer at the sharp vertex of the flat-end probe promotes the formation of small vorticities that detached approximately 12 mm from the base of the flat-end cylindrical probe and transported downstream. Vortex shedding, indicated with an arrow, occurs at a frequency of 10 Hz.

In figs. 3 b) and 3 e), corresponding to a velocity of 0.4 m/s, the boundary layer separation forms a larger wake than that observed in fig. 3 d). It can be observed that separation and a recirculation zone are generated up to 12 mm from the base of the probe as shown in the streamline map and the velocity field. The velocity fields show that the water boundary layer at the sharp vertex of the flat-end probe promotes the formation of small vorticities that are detached approximately 12 mm from the base of the specimen and transported downstream. The frequency of vorticity detachment (15 Hz) is greater compared to the case with a velocity of 0.2 m/s.

In figs. 3 c) and 3 f), corresponding to a velocity of 0.6 m/s and isothermal conditions, the velocity field obtained with the PIV measurements and the streamlines show that there is an area of high vorticity, that is, there are vortices that spin in opposite directions and cause the recirculation zone to fluctuate between 9 and 13 mm in length; vortex shedding is detached at a frequency of 24 Hz and is more notorious than in the other cases. The vortex shedding point is indicated by an arrow in the image of the streamlines; this point if further downstream than in the two previous cases.

Fig. 4 shows the results obtained under non-isothermal conditions (probe heated to 915 °C and rapidly cooled inside a plexiglass tube with water at 60 °C). At a velocity of 0.2 m/s, there is no separation of the boundary layer in the leading edge of the flat-end probe nor can vortex shedding be seen during stable film boiling anywhere along the probe surface. Furthermore, streamlines characteristic of laminar flow can be seen (see fig.4 a)). The pressure generated by the vapor film around the entire probe surface compensates for the pressure gradient that could cause separation of the boundary layer due to the interaction fluid-probe.

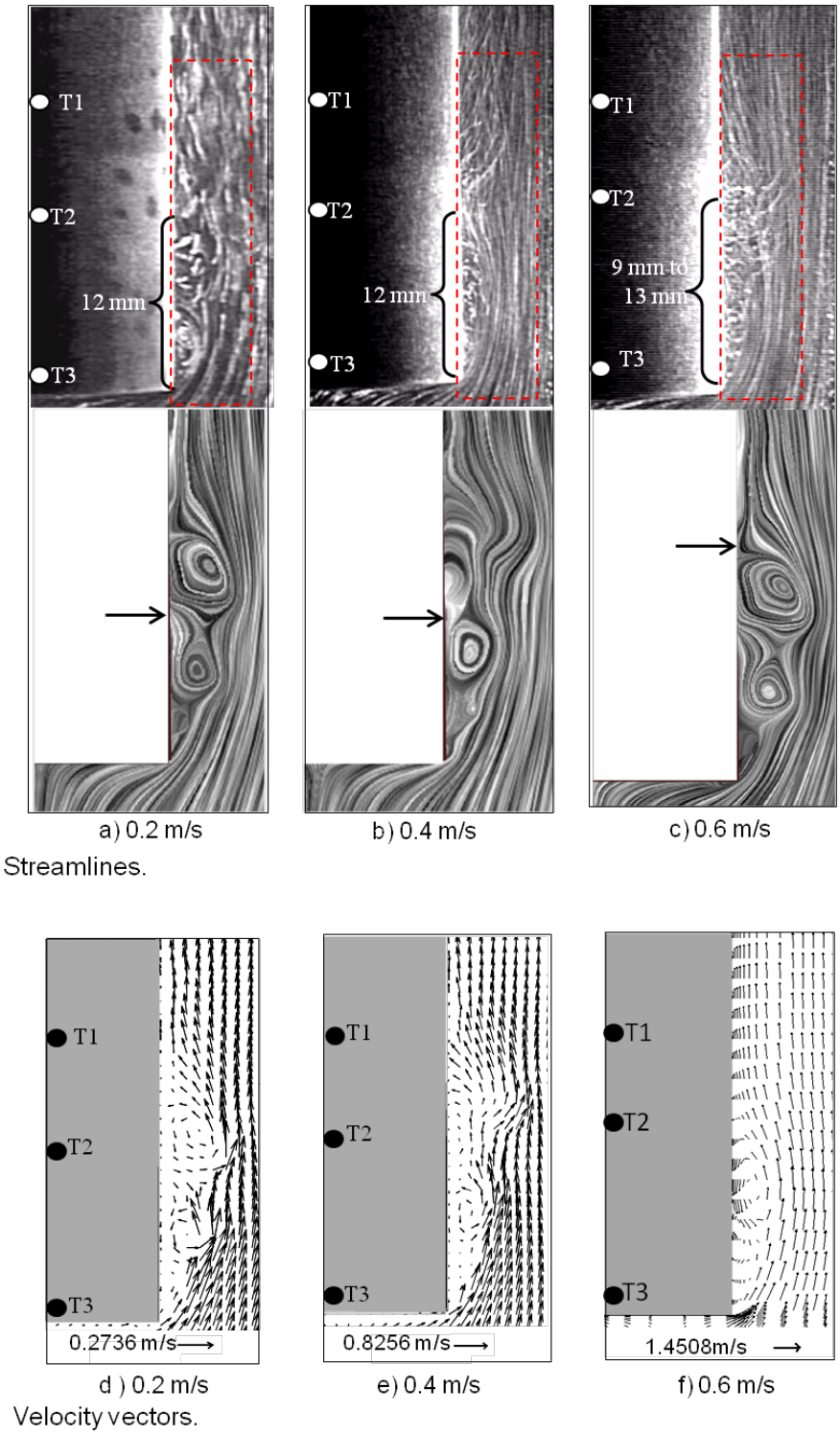

Fig. 3. Streamlines and velocity fields around the flat-end cylindrical probe for the three free stream values of water velocity studied (0.2, 0.4 and 0.6 m/s) under isothermal conditions, and 1.2 seconds after the flat-end cylindrical probe reached the work position.

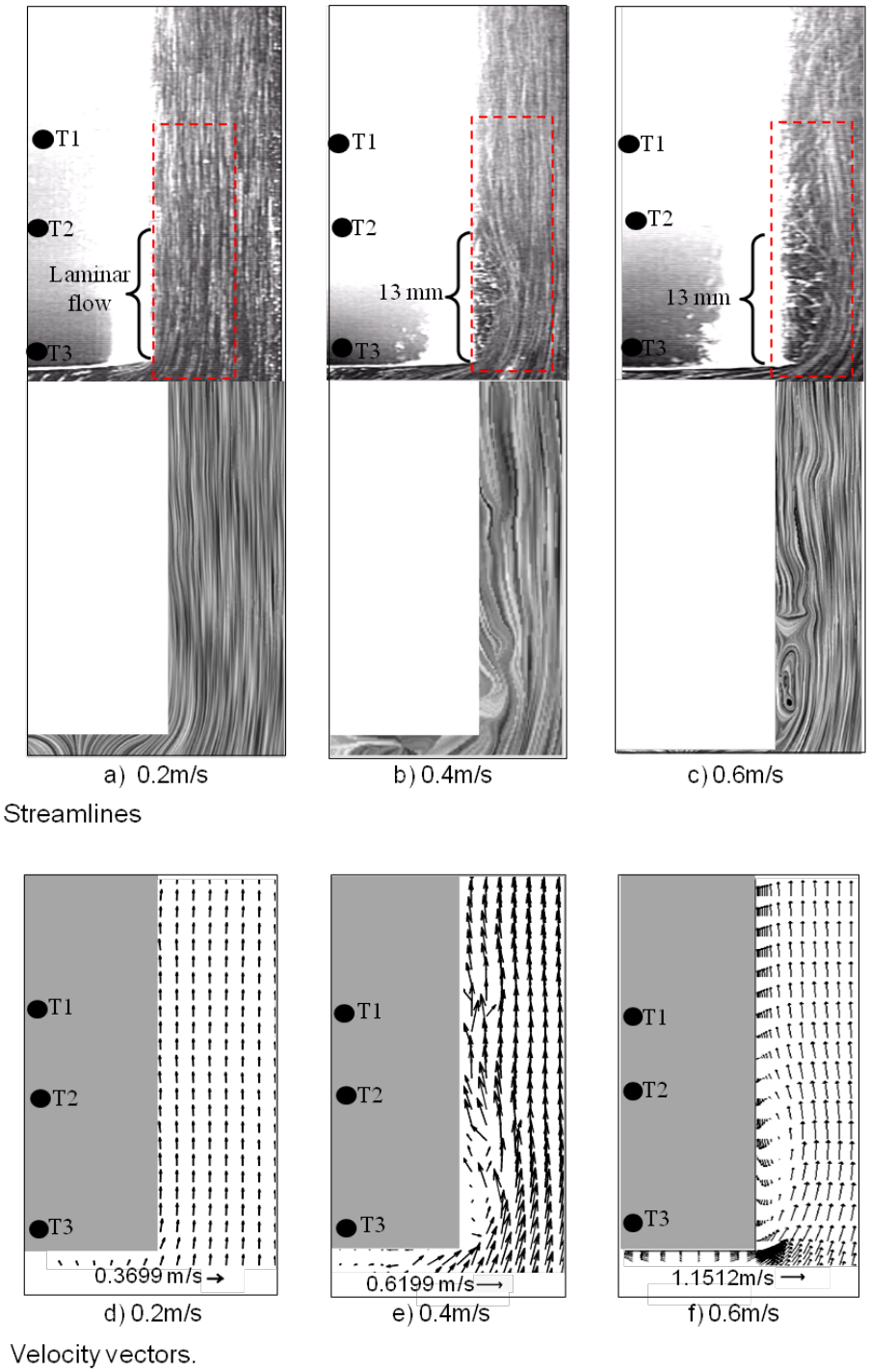

Fig. 4. Streamlines and velocity fields around the flat-end cylindrical probe for the three free stream values of water velocity studied (0.2, 0.4 and 0.6 m/s) under non-isothermal conditions, and 1.2 seconds after the flat-end cylindrical probe reached the work position.

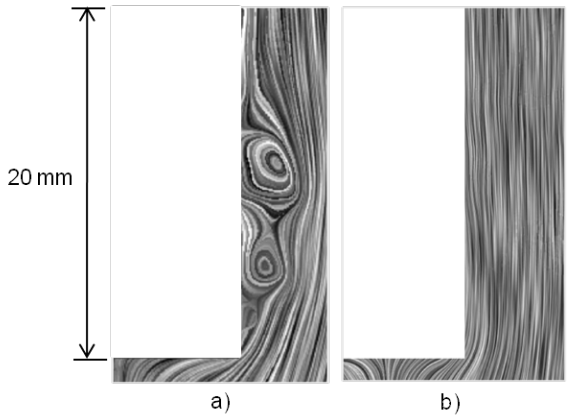

Fig. 5. Computed streamlines around the flat-end cylindrical probe with a free stream velocity of 0.2 m/s: a) isothermal and b) non-isothermal conditions (quenching of the probe with an initial temperature of 900ºC).

The vector velocity field around the flat-end cylindrical probe show a laminar flow (see fig. 4 d)), favoring the formation of a very stable vapor blanket around the flat-end cylindrical probe.

In the case of a free-stream water velocity of 0.4 m/s, an area of instability can be observed within the vapor film (see fig. 4 b) and 4 e)), caused by an increase in the drag force. This instability may be confused with shedding of the boundary layer. However, through analysis of the video-recordings and the velocity field around the probe, it was observed that the instability of the vapor film at the base of the probe is a result of vapor drag by water when the free-stream water velocity increases from 0.2 to 0.4 m/s. It is important to note that the velocity vectors further up from the instability area on the probe are laminar and a vortex shedding point is not seen nor formation of wakes, favoring the formation of a stable vapor blanket around the probe in this zone.

Under non-isothermal conditions and a velocity of 0.6 m/s the flow around the probe is highly turbulent and with vapor dragged at the recirculation zone formed due to an adverse pressure gradient on the side, close to the base of the probe. However, no separation of the boundary layer is observed. Consequently, there is no shedding of vortices downstream (see figs. 4 c) and 4 f)).

The above results show that fluid dynamics around the probe under non-isothermal conditions, in which case a vapor film is present during relatively long times (with respect to the total quench time), is very different from that observed under isothermal conditions.

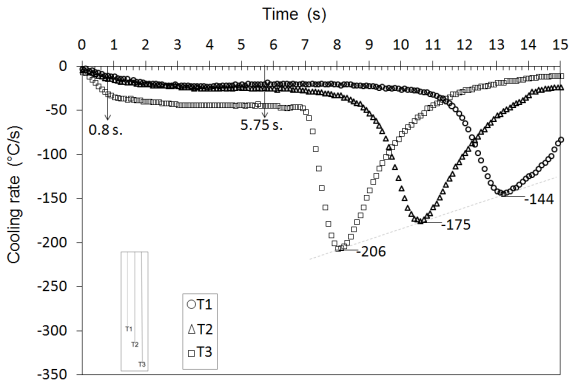

Fig. 6. Local cooling rate curves, as a function of time, for the flat-end cylindrical probe cooled from 900 °C with water at 60ºC flowing at a velocity of 0.2 m/s. The numbers near the maxima are cooling rate values which occur at 7.5, 9.7 and 11.7 s, respectively.

This is confirmed in fig. 5 which shows computed streamlines (by the Line Integral Convolution (LIC) technique) under isothermal (fig. 5 a)) and non-isothermal (fig. 5 b)) conditions, at constant free-stream water velocity (0.2 m/s), near the base of the probe. Fig 5 a) shows a recirculation zone originated by the dynamic boundary layer separation, inside which small vortices are formed. On the other hand, under non-isothermal conditions (fig. 5 b)) there is no boundary layer separation and laminar flow can be seen.

3.2 Cooling rate curves

Fig. 6 shows local cooling rate curves computed from the thermal histories measured with the three thermocouples inserted in the probe (refer to fig. 2). They correspond to an experiment with the probe heated to 900 ºC and cooled in water at 60 °C flowing at a free-stream velocity of 0.2 m/s. Analysis of the cooling rate curves for each of the thermocouple positions shows that the cooling rate curves remain fairly horizontal during the film boiling stage due to the stability of the vapor film formed along the probe surface (refer to figs. 4 a) and 5b)). Thermocouples T1 and T2 show very similar cooling rate values during the first 5.75 s. In contrast, the curve for thermocouple T3 shows a higher cooling rate which may be related to the fact that, being this thermocouple closer to the base of the probe, the start of the collapse of the film boiling at the base of the probe was occurs earlier, approximately at 5.75 seconds.

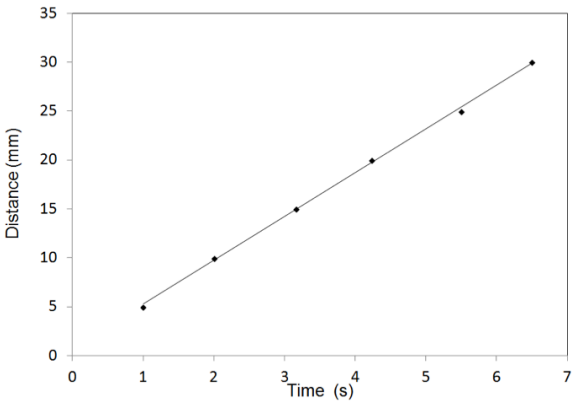

Fig. 7. Wetting front position during cooling of the flat-end cylindrical probe cooled from 900 °C with water at 60 °C at a velocity of 0.2 m/s.

Some researchers have claimed, based on their experiments, that the wetting front starts at the base of the flat-ended cylindrical probe, but does not ascend with angular symmetry (even for a fully developed flow and low cooling rate values). Additionally, they attribute this behavior to fluid dynamics in the vicinity of the base of the probe, mainly to the existence of vorticities (Vergara-Hernández, and Hernández-Morales, 2009). However, the streamlines and velocity field for 0.2 m/s, under non-isothermal conditions, show that the disturbances in the vapor film are very small, which rules out the presence of vorticities in the base of the probe (refer to figs. 4 a), 4 d) and 5 b)), however under isothermal conditions, at the same velocity, vorticities are present (refers to figs. 3 a), 3 d) and 5 a)).

The three cooling rate curves show maxima that are associated with the wetting front passing in front of each one of the thermocouple locations. Do keep in mind that the curves were computed from thermal histories measured within the probe and, therefore, are lagging with respect to the surface thermal histories. In fig. 6 it may be observed that, even though the cooling rate curves have different shapes, the maximum values are approximately equally spaced in time and decrease from -206 °C/s for T3 to -144 °C/s for T1. This is the result of a wetting front that moves upward at a constant velocity, as seen in fig. 7, which is a plot of six values of the wetting front location and its corresponding time, as determined from the video-recordings, for a probe cooled in water at 60 ºC flowing with a free-stream velocity of 0.2 m/s; the data corresponds to increments of 10 mm from the base of the probe.

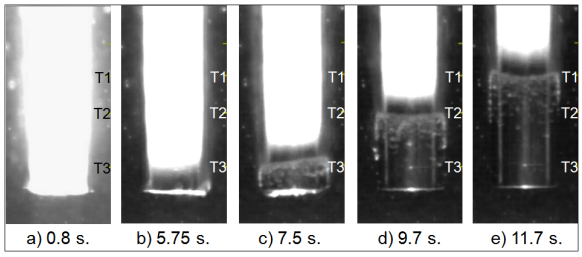

Fig. 8. Photographs recorded with the high-speed camera, without using wave-length filters, showing the evolution of the wetting front during cooling of the flat-end cylindrical probe from 900 °C with water at 60ºC flowing at 0.2 m/s.

The fact that the wetting front moves with a constant velocity is characteristic of the experimental system used in this work; the wetting front velocity, as it will be shown below, is a function of the Reynolds number.

In fig. 8 several images extracted from the high-speed camera video-recordings are shown for an experiment with water flowing at 0.2 m/s under non-isothermal conditions. The formation and collapse of the vapor film as well as the advance of the wetting front up to the position of thermocouple T1 are shown. The wetting front moves symmetrically on its angular component around the probe. Clearly, there is a small zone ahead of the wetting front that is significantly cooler than the rest of the probe.

The local cooling rate curves at the thermocouple positions (refer to fig. 2) during rapid cooling from 900 ºC in water at 60 °C flowing at 0.4 m/s are shown in fig. 9. In contrast with the results with a free-stream water velocity of 0.2 m/s, an analysis of the cooling rate curves in the stable vapor regime shows different cooling rate values for T1 and T2, due to an increase in heat extraction, causing a reduction in the re-wetting time from 5.75 seconds to 4.93 seconds for water flowing at 0.2 and 0.4 m/s, respectively. The higher heat extraction rate is due to the transition from laminar to turbulent flow patterns around non-isothermal the probe.

Note that the behavior of thermocouple T3 is similar to that observed during cooling with water flowing at 0.2 m/s. This is because disturbances in the vapor film are very small. Also, from fig. 9, the curves have staggered maximum values of -203, -190, and -144 °C/s, which correspond to a wetting front moving at a constant velocity as observed in fig. 10.

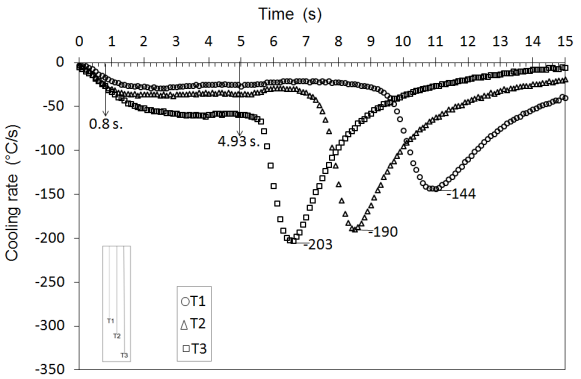

Fig. 9. Local cooling rate curves of the flat-end cylindrical probe cooled from 900 °C with water at 60ºC flowing at 0.4 m/s. The numbers near the maxima are cooling rate values which occur at 5.9, 7.9 and 9.8 s, respectively.

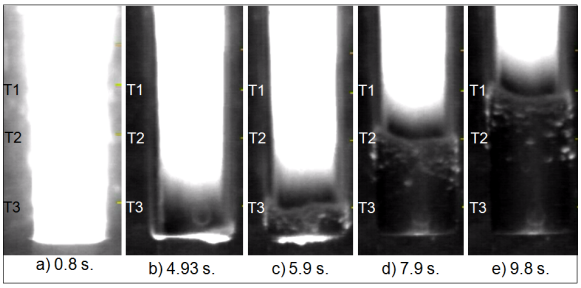

Fig. 10. Photographs recorded with the high-speed camera, without using wave-length filters, showing the evolution of the wetting front during cooling of the flat-end cylindrical probe from 900 °C with water at 60ºC flowing at 0.4 m/s.

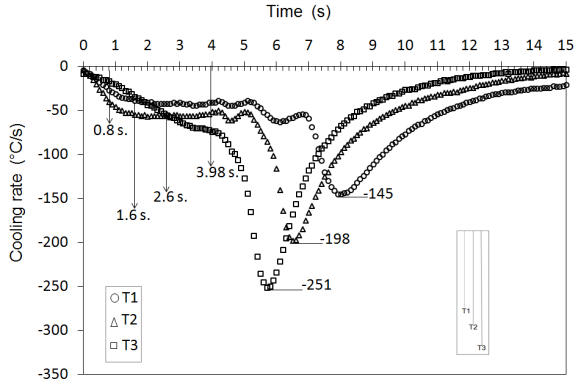

Fig. 11. Local cooling rate curves of the flat-end cylindrical probe cooled from 900 °C with water at 60ºC flowing at 0.6 m/s. The numbers near the maxima are cooling rate values which occur at 5.1, 5.8 and 7.2 s, respectively.

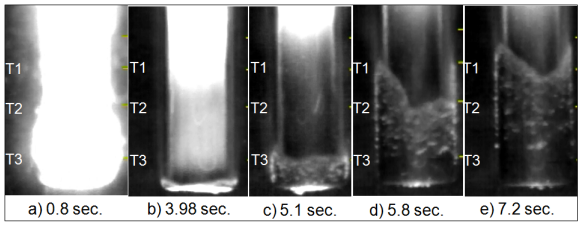

Fig. 12. Photographs recorded with the high-speed camera, without using wave-length filters, showing the evolution of the wetting front during cooling of the flat-end cylindrical probe from 900 °C with water at 60ºC flowing at 0.6 m/s.

Fig. 11 shows local cooling rate curves for the three thermocouples (refer to fig. 2) during rapidly cooling in water flow at 60 °C flowing at 0.6 m/s. Under these experimental conditions it is observed that the vapor film at the positions of thermocouples T1 and T2 is established at 1.6 seconds, while the vapor film at the thermocouple position T3 is never fully established (see cooling rate values at 0.8, 1.6, and 2.6 seconds). That is, it does not reach a constant cooling rate value. The vapor film collapses at the base of the cylinder at 3.98 seconds, unlike the experiment with water flowing at 0.4 m/s where it collapses at 4.93 seconds. Once the vapor film collapses at the base of the probe, the boundary layer is destabilized and vortices are generated that destabilize the vapor film and cause oscillations in the cooling rate curves of the thermocouples furthest from the base (T1 and T2).

Fig. 12 shows images of the vapor film evolution around the probe during rapidly cooling in water flow at 60 °C flowing at 0.6 m/s as observed without using optical filters. Under these video-recording conditions the vapor film expands at the base of the probe due to vapor drag (fig. 12 a)). Expansion of the vapor film in this area is related to the recirculation zone at the base of the probe induced by the inertial forces and the adverse pressure gradient near the base of the probe, diminishing heat extraction in that zone. Therefore, the vapor film is always unstable and the local cooling rate curve calculated for thermocouple T3 (refer to fig. 11) does not show a horizontal region, as is the case for T2 and T1.

When 3.98 seconds have elapsed, the vapor film collapses at the base of the probe and the wetting front forms (see fig. 12 b)). However, fluid velocity remains constant and causes the vapor film in an area around the location of thermocouple T3 to thin more quickly with respect to areas around thermocouples T1 and T2.

Table 2. Average wetting front velocity.

Condition	Wetting front velocity
0.2 m/s	4.64×10^{-3} m/s
0.4 m/s	5.61×10^{-3} m/s
0.6 m/s	11.59×10^{-3} m/s

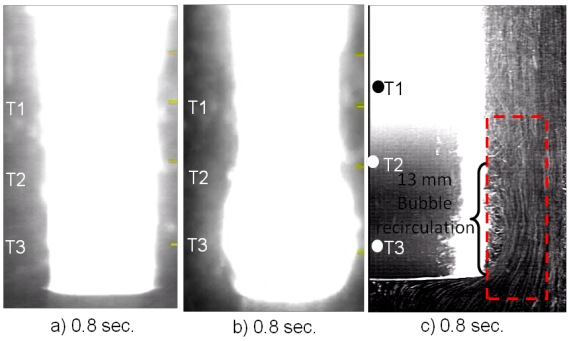

Fig. 13. Film boiling formed during cooling of the flat-end cylindrical probe from 900 ºC with water at 60 ºC. Without using the light wavelength filter and a water velocity of a) 0.4 m/s and b) 0.6 m/s; c) using the light wavelength filter and a water velocity of 0.6 m/s.

According to fig. 12 c), the vapor film has collapsed after 5.1 seconds; later on, the wetting front rises non-symmetrically, as observed in figs. 12 d) and 12 e).

The wetting front velocity, the loci of the boundary between the vapor film and the occurrence of nucleate boiling, obtained from figs. 8, 10 and 12, for each one of the conditions studied, 0.2, 0.4 and 0.6 m/s, is shown in table 2. Upon increasing water velocity, the wetting front velocity increases.

The vapor blanket drag effect for high Reynolds numbers can be assessed with the help of figs. 13 a) and b) which shows images taken without the light filter and two values of the free-stream water velocity: 0.4 and 0.6 m/s, respectively. When the water flows at 0.4 m/s (see fig. 13 a)) there is no expansion of the vapor film as the value of the Reynolds number is not sufficiently large to produce significant disturbance. In contrast, when the water free-stream velocity reaches 0.6 m/s (see fig. 13 b)), local expansion of the film boiling near the base of the probe is clearly observed with the light filter and the macro lens (see fig. 13 c), which is produced by the recirculation zone that is generated at the base of the flat-end probe.

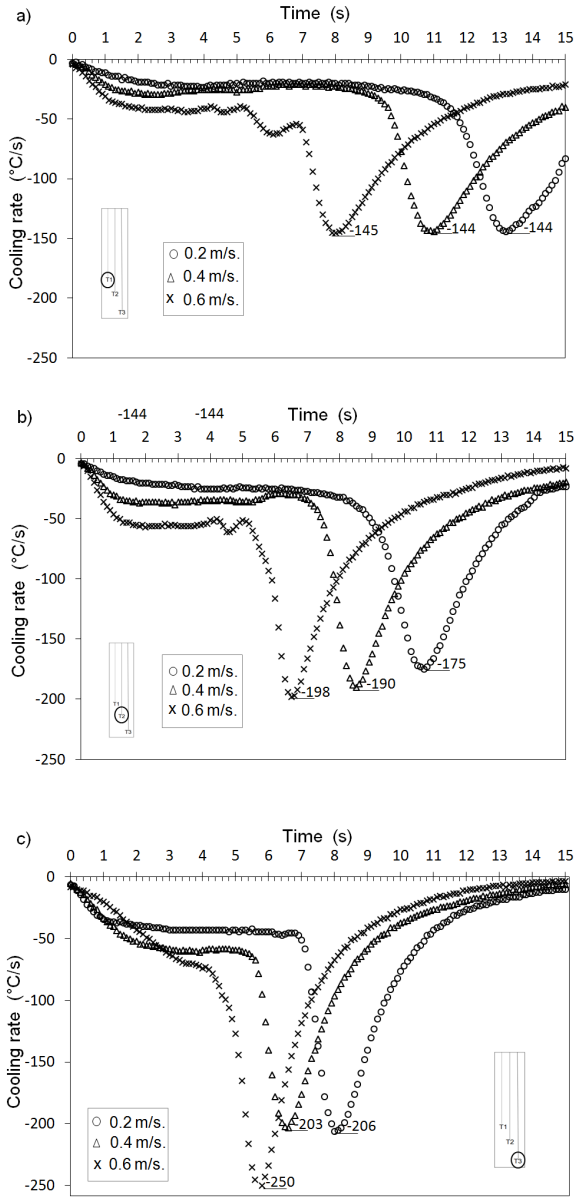

Fig. 14. Local cooling rate curves at each one of the thermocouple positions during cooling of the flat-end cylindrical probe from 900 °C with water at 60ºC and the three different velocities used in this study: a) T1, b) T2 and c) T3.

As mentioned earlier, the light filter was used to block light with wavelengths greater than 550 nm, characteristic of probes at around 900 °C which, therefore, permits clear visualization of the streamlines even at high temperatures.

Fig. 14 shows cooling rate curves for the three water free stream velocities studied at the thermocouple position T3. Upon increasing the water

velocity from 0.2 to 0.4 m/s, the cooling rate during the existence of the vapor film increases and the duration of the vapor film decreases. In the film boiling stage there is a period of time during which the cooling rate remains almost constant. However, by increasing the water velocity to 0.6 m/s, it is observed that the cooling rate associated with the vapor film in the first 1.8 seconds of the experiment is lower than that corresponding to free-stream water velocities of 0.2 and 0.4 m/s, and it stays below the cooling rate corresponding to 0.4 m/s, until the 3-second mark. This confirms that in the first few seconds of the experiment, the vapor blanket expands near the base of the probe at a water velocity of 0.6 m/s, which decreases the local cooling rate. Also, during the film boiling stage a constant cooling rate is not observed, which confirms that the vapor blanket around the position of the thermocouple T3 is not stable for a free-stream water velocity of 0.6 m/s.

Three interesting features are observed when comparing the curves in fig. 14: 1) the only case in which there is no evidence of a stable film boiling is for T3 with water flowing at 0.6 m/s; 2) the highest water velocity studied (0.6 m/s) causes oscillations in the cooling curves corresponding to T1 and T2; and 3) the difference in the cooling rate value during the film boiling stage between the curves for water flowing at 0.4 and 0.6 m/s is largest for T3 and negligible for T1. Also, the maximum cooling rate is rather independent of the free-stream water velocity for T1.

Conclusions

Using visualization techniques of video-recordings with a high-speed camera and light filters while simultaneously measuring local thermal histories, the flow structure generated during forced convective quenching of a laboratory-scale around flat-end cylindrical probes with an initial temperature of 900 ºC, rapidly cooled in water at 60 ºC flowing at three different velocities (0.2, 0.4, and 0.6 m/s) was characterized. From the results, the following conclusions were obtained:

1. The flow structure around the probe under non-isothermal conditions is markedly different from that observed under isothermal conditions. Therefore, it is not correct to correlate fluid dynamics measured around metallic probes under isothermal conditions with the behavior of local cooling rate curves.

2. The boundary layer shedding phenomenon, generated when water flowing at 60 ºC and 0.2 m/s impacts the flat face of a cylindrical probe at room temperature, it is not observed in experiments under non-isothermal conditions due to the formation of a stable film boiling which compensates the adverse pressure gradient area generated when the boundary layer is shed.

3. When a flat-end cylindrical probe with a temperature of 900 °C is submerged in water at 60 °C flowing at 0.6 m/s, the vapor film is perturbed by vapor drag resulting from the interaction between the fluid and the base of the probe. Specifically, this drag is produced by the change in direction of the liquid upon impact with the base of the probe. Once the vapor film collapses, the boundary layer is shed and wakes that further destabilize the film boiling are formed.

4. The flat-end cylindrical probe is a good choice to conduct cooling curve studies, provided the Reynolds number is below 37000 (the value of the Reynolds number corresponding to a free-stream water velocity of 0.4 m/s in the equipment used).

5. One of the most important contributions of this paper to understand boiling phenomena during forced convective quenching of laboratory-scale probes is to show that the presence of the vapor film delays the separation of the boundary layer. That is, increasing the Reynolds number results in vapor drag on the probe surface which delays separation of the boundary layer until the vapor film on the surface of the probe collapses.

Acknowledgements

We acknowledge the financial support provided by CONACyT through grant number 131720, as well as the financial support to A. Cervantes-García to conduct his graduate studies.

We also thank UMSNH, ITM, UNAM and SNI for their permanent support to the academic research network on Mathematical Simulation of Materials Processing and Fluid Dynamics.

Abbreviations

ISO	International Organization for Standardization
ASTM	American Society for Testing and Materials
JIS	Japanese Industrial Standards
AISI	American Iron and Steel Institute
LIC	Line Integral Convolution
T1	thermocouple 1
T2	thermocouple 2
T3	thermocouple 3

References

ASTM D6200-01. (2012). Standard test method for determination of cooling characteristics of quench oils by cooling curve analysis. *Annual Book of ASTM Standards, ASTM International*. West Conshohocken, PA.

ASTM D6482-06. (2011). Standard test method for determination of cooling characteristics of aqueous polymer quenchants by cooling curve analysis with agitation (Tensi Method). *Annual Book of ASTM Standards, ASTM Inter- national*. West Conshohocken, PA.

ASTM D6549-06. (2011). Standard test method for determination of cooling characteristics of quenchants by cooling curve analysis with agitation (Drayton Unit). *Annual Book of ASTM Standards, ASTM International*. West Conshohocken, PA.

ASTM D7646-10. (2010). Standard test method for determination of cooling characteristics of aqueous polymer quenchants for aluminum alloys by cooling curve analysis. *Annual Book of ASTM Standards, ASTM International*. West Conshohocken, PA.

Bodin, J. and Segerberg, S. (1992). Measurement and evaluation of the quenching power of quenching media for hardening. *Quenching and Distortion Control*, 1-12.

Hernández-Morales, B., *et al*. (2011). Experimental and computational study of heat transfer during quenching of metallic probes. *INTECH Open Access Publisher*, 49-72.

Hernández-Morales, B., Vergara-Hernández, H. J. and Solorio-Díaz, G. (2011). Fluid dynamics during forced convective quenching of flat-end cylindrical probes. *Proceedings of the WSEAS International Conference on Heat and Mass Transfer (HMT 11)*, 135-141.

ISO 9950. (1995). Industrial quenching oils determination of cooling characteristics nickel-alloy probe test method. *International Organization for Standardization*, Geneva, Switzerland.

JIS K2242. (2012). Heat treat fluids. *Japanese Standards Association*, 4-1-24, Akasaka, Minato-ku, Tokyo 107-8440, Japan.

Kern, R. (1985). Distortion and cracking. II.– Distortion from quenching. *Heat Treat 27*, 41-45.

Kobasko, N. I., *et al*. (1997). Experimental determination of the first and second critical heat flux densities and quench process characterization. *Journal of Materials Engineering and Performance 6*, 93-101.

Kunzel, T. H., Tensi, H. M., Welzel, G. (1986). Rewetting rate-the decisive characteristic of a quenchant (retroactive coverage). In *5th International Congress on Heat Treatment of Materials 3*, 1806-1813.

Leidenfrost, J. G. (1756). *De Aquae Communis Nonnullis Qualitatibus Tractatus*. Ovenius.

Long G. F. (1994). Control of quenching distortion in gears. *Jinshu Rechuli 5*, 39-40.

López-Martínez E., Hernández-Morales J.B., Solorio-Díaz G., Vergara-Hernández H.J., Vázquez-Gómez O. and P. Garnica-González. (2013). Prediction of hardness profiles in medium and low carbon steel Jominy probes. *Revista Mexicana de Ingeniería Química 12*, 609-619.

Lübben, T., Frerichs, F. and Zoch., H.W. (2011) Rewetting behaviour during immersion quenching. *Strojarstvo: Časopis za Teoriju i Praksu u Strojarstvu 53*, 45-52.

Maniruzzaman, M. and Sisson, R. D. (2001). Bubble dynamics during quenching of steel. *21st ASM Heat Treating Society Conference*, 104-11.

Narazaki, *et al*. (2004). Development of new sliver probe for cooling power test of polymer quenchants. 14th *Congress of International*

Federation for Heat Treatment and Surface Engineering.

Narazaki, M., Totten. G.E and G.M. Webster. (2002). Hardening by reheating and quenching. *Handbook of Residual Stress and Deformation of Steel*, 11-12.

Narazaki, M., *et al*. (1996). Laboratory test of cooling power of polymer quenchants. *ASM International*. Materials Park, OH (United States).

Narazaki, M., Fuchizawa, S. and Usuba, M. (1989). Effects of specimen geometry on characteristic temperature during quenching of heated metals in subcooled water. *Tetsu-to-Hagane (J. Iron Steel Inst. Jpn.) 75*, 634-641.

Nukiyama and Shiro. (1966). The maximum and minimum values of the heat Q transmitted from metal to boiling water under atmospheric pressure. *International Journal of Heat and Mass Transfer 9*, 1419-1433.

Owaku, S. (1992). Quench distortion of steel parts. *Journal of the Japan Society for Heat Treatment 32*, 198-202.

Ramezanzadeh H., Ramiar A. and Yousefifard M. (2017). Numerical investigation into coolant liquid velocity effect on forced convection quenching process. *Applied Thermal Engineering*, http://dx.doi.org/10.1016/j.applthermaleng.2017.05.008

Sang L., Jinsub K. and Jungho L. (2017). Boiling heat transfer of forced immersion quenching on hot steel block. *Proceedings of the Asian Conference on Thermal Sciences 2017*, 1st ACTS, March 26-30,2017, Jeju Island, Korea. ACTS-P00167.

Shiro and Nukiyama. (1984). The maximum and minimum values of the heat Q transmitted from metal to boiling water under atmospheric pressure. *International Journal of Heat and Mass Transfer 27*, 959-970.

Smoljan B. (2006). Prediction of mechanical properties and microstructure distribution of quenched and tempered steel shaft. *Journal of Materials Processing Technology 175*, 393-397

Stich, A. and Tensi, H. M. (1995). Heat transfer and temperature distribution with wetting process during immersion quenching. *Harterei-Technische Mitteilungen (Germany) 50*, 31-34.

Tensi, H.M., and Steffen, E. (1985). Measuring of the quenching effect of liquid hardening agents on the basis of synthetics. *Steel Res 56*, 9, 489-495.

Tensi, H.M., Stich, A. and Totten, G.E. (1995). Fundamentals of quenching. *Metal Heat Treating 3/4*, 20-28.

Tensi, H. M. and Stich, A. (1992). Martens hardening of steel-Prediction of temperature distribution and surface hardness. *Materials Science Forum, Trans Tech Publications*, 741-754.

Tensi, H. M., Totten,G. E. and Webster G.M. (1997). Proposal to monitor agitation of production quench tanks. *Heat Treating: Including the 1997 International Induction Heat Treating Symposium-Proceed*. 17th Conf., D.l. Milam, D.A. Poteet, G.D. Pfaffmann, V, Rudnev, A Muehlbauer, and W.B. Albert, Ed., ASM International 1997. 423-441.

Tensi, H. M. Totten, G. E. and Kunzel, T. (2000). Physics and technology of quenching in fluids. I. Physics of quenching. In 20th *ASM Heat Treating Society Conference*, 727-730.

Thielicke W. and Stamhuis E. J. (2014). PIVlab -time-resolved digital particle image velocimetry tool for MATLAB (version:1.32). http://dx.doi.org/10.6084/m9.figshare.1092508

Totten, G. E., Bates, C. E., and Clinton, N. A. (1993). Chapter 3-Cooling curve analysis. *Handbook of Quenchants and Quenching Technology, ASM International, Materials Park*, OH, 69-128.

Totten, G. E., *et al*. (2009). Quenchant characterization by cooling curve analysis. *Journal of ASTM International 6*, 1-29.

Vergara-Hernández, H. J. and Hernández-Morales, B. (2009). A novel probe design to study wetting front kinematics during forced convective quenching. *Experimental Thermal and Fluid Science 33*, 797-807.

Vergara-Hernández, H.J., Hernández-Morales, B. and Solorio-Díaz, G. (2010). Effect of the hydrodynamic conditions on the vapor film during forced convective quenching. 18th *International Federation for Heat Treatment and Surface Engineering* Congress, Rio of Janeiro, Brazil, July 26th - 30th, 5187-5195.